THESIS FOR THE DEGREE OF LICENTIATE OF ENGINEERING

Advanced Nanofabrication for Novel Plasmonic Biosensors

FRANCESCO MAZZOTTA

Department of Applied Physics
Chalmers University of Technology
Göteborg, Sweden 2012

Advanced Nanofabrication for Novel Plasmonic Biosensors
FRANCESCO MAZZOTTA

Department of Applied Physics
Chalmers University of Technology
SE-412 96 Göteborg
Sweden
Telephone +46(0)31-772 6109
E-mail: mazzotta@chalmers.se

Cover illustration: on the left side, a cross section of one of the photo diodes with gold nanodisks used as biosensor in Paper I; on the right side, a schematic illustration of a nanofluidic membrane with gold nanoplasmonic particles located onto the inner walls of the nanochannels.

Printed at Chalmers Reproservice
Göteborg, Sweden 2012

Contents

List of Abbreviations **iii**

Abstract **iv**

Appended Papers **v**

1 Introduction **1**

2 Nanoplasmonics **7**

2.1 Introduction to nanoplasmonics 7

2.2 Probing nanoplasmonics 10

2.3 Nanoplasmonics for sensing 12

3 Nanofabrication as a toolbox **14**

3.1 Characterization at the nanoscale 14

3.1.1 Scanning electron microscope (SEM) 15

3.1.2 Atomic force microscope (AFM) 17

3.1.3 Ellipsometry 18

3.2 Fabrication at the nanoscale 18

3.2.1 Photolithography 20

3.2.2 Colloidal lithography and Hole-mask Colloidal lithography (HCL) 21

3.2.3 Ion milling 24

3.2.4 Reactive Ion Etching (RIE) 24

3.2.5 Wet etching 25

3.2.6 Electron beam assisted evaporation 25

3.2.7 Low pressure chemical vapor deposition (LPCVD) and Plasma enhanced chemical vapor deposition (PECVD) 27

4 Summary and outlook **28**

4.1 Summary of Papers 28

4.2 Conclusions and outlook 28

Acknowledgments **31**

List of Abbreviations

AFM	atomic force microscope
BSE	backscattered electrons
CVD	chemical vapor deposition
DDA	discrete dipole approximation
ELISA	enzyme-linked immunosorbent assay
FDTD	finite-difference time domain
hCG	human chorionic gonadotrophin
HCL	hole-mask colloidal lithography
LED	light emitting diode
LPCVD	low pressure chemical vapor deposition
LSPR	localized surface plasmon resonance
PCR	polymerase chain reaction
PECVD	plasma enhanced chemical vapor deposition
PMMA	polymethyl methacrylate
PVD	physical vapor deposition
QCM	quartz crystal microbalance
RF	radio frequency
RIE	reactive ion etching
SE	secondary electrons
SEM	scanning electron microscope
SPR	surface plasmon resonance

Abstract

There is an increasing interest in the development of novel biosensors in the foreseeable future. The impact on society of diseases connected to the aging of population, for example infectious diseases, cancer and Alzheimer's disease, has the potential of increasing the running costs of welfare over a sustainable threshold already within a few years. Early diagnostics and point-of-care testing will play a fundamental role in achieving a cost-effective health-care capable of satisfying the increasing needs. This translates into a drive towards further improved diagnostic devices where miniaturization and enhanced performances enabling detection of low-abundant biomarkers is expected a key component.

In this thesis work, the aim has been to translate advanced nanotechnology fabrication processes to novel biosensor platforms which could address some of the key issues just presented above.

In order to achieve this, a sensing principle suitable for employment in miniaturized devices is necessary. In this work, we exploited the sensitivity of the optical properties of metal nanoparticles to changes in refractive index of the surrounding environment. Such nanoplasmonic structures enable a transduction of biorecognition events occurring within a few tens of nanometers from their surface into a detectable optical contrast, or color.

The inherent flexibility of nanofabrication processing combined with the size and simple instrumentation of nanoplasmonic based transducers allows for a wide variety of potential applications. In this work, two novel biosensing platforms were developed addressing two different challenges: on the one hand, the development of a portable and simple device for point-of-care diagnostics, and on the other hand, a sensor with potential to effectively tackle the challenge of detecting low-abundant analyte in small volumes.

In the first case, the sensor and detector elements were integrated into the same chip by fabricating gold nanostructures directly onto photodiodes. In this way, biorecognition events could be directly transduced into electric signals via shifts in the photocurrent generated by the detectors. The sensor was tested by detection of specific protein binding in a custom made flow cell.

In the second case, steps towards the development of a biosensing platform for detection of low concentration of biomarkers in small volumes were taken by developing a fabrication process which integrates gold nanoplasmonic structures in a nanofluidic network. By locating the sensor elements directly into nanofluidic channels, target molecules can be efficiently transported from the bulk to the sensor surface. We believe that this could enable combined high capture efficiency, short detection time and low sample consumption even at low concentration of analytes.

Keywords: *Localized surface plasmon resonance, Biosensor, Bioanalytical sensing, Nanodisks, Photo diode, Solar cell, Nanofabrication, Nanoplasmonics, Nanopores.*

Appended Papers

Paper I

Nanoplasmonic biosensing with on-chip electrical detection

Mazzotta, Francesco, Guoliang Wang, Carl Hägglund, Fredrik Höök and Magnus P. Jonsson
Biosensors & bioelectronics, **26** (4), 1131-6, (Dec 2010).

My contribution: I was responsible for planning and designing the experimental work together with MJ, I performed the main part of the experiments. I wrote part of the manuscript.

Paper II

High Throughput Fabrication of Plasmonic Nanostructures in Nanofluidic Pores for Biosensing Applications

Mazzotta, Francesco, Fredrik Höök and Magnus P. Jonsson
Submitted

My contribution: I was responsible for planning and designing the experimental work, I performed all the experiments. I wrote the main part of the manuscript.

1 Introduction

A bioanalytical sensor, or biosensor, is a device capable of detecting suspended analytes, often referred to as target molecules, by means of a physical/chemical transduction principle. Among different types of biosensors, one important category is surface-based, where the signal is generated from biorecognition reactions occurring at the interface between the detector element and the sample. In a typical surface-based biosensor, a more or less complex sample is placed in contact with the surface of the device, on which a pre-defined set of reactions is allowed to occur. Specific binding of a target molecule is ensured by having receptor molecules, often referred to as probe molecules, immobilized on the surface. The biorecognition reaction is then converted into a detectable signal by means of a transducer principle which can be based on different physical principles, such as optical[1–5], electrochemical[6–8], thermometric[9,10], magnetic[11,12], piezoelectric.[13–15] The transducer principle should be chosen such that it is sensitive enough to, within reasonable time scales, detect as low surface coverage of target as possible on the sensor surface. This minimum surface coverage of target molecules required to generate a detectable signal, i.e. a signal which is larger than noise floor, determines the **sensitivity** of a sensor and consequently its limit of detection with respect to target concentration in the sample. In other words, the sensitivity of a sensor corresponds to the amount of bound target molecules necessary to generate a detectable response.

While a high sensitivity is generally perceived as its most important component, a useful biosensor must also ensure that only a specific set of target molecules binds. In fact, the contribution to the signal from molecules not of interest has merely the effect of increasing the background and decreasing the reproducibility of the measurements. The discrimination between different recognition events determines the **selectivity** of a sensor. This is ensured by careful selection of probe molecules and the means by which they are immobilized on the sensor surface.

Moreover, the target molecules of interest must reach the surface of the sensor in an efficient way, since the rate of binding depends strongly on the means of **transport**, especially in samples with slowly diffusing analyte present in small quantities. To accomplish this, **miniaturization** of the devices is often used in combination with microfluidics, which decreases the minimum sample volume required to operate at sufficient transport conditions. This has led to the development of diverse liquid-handling strategies, such as flowing the sample over the sensor[16], through the sensor[17], or even drying it on top of the detector.[18]

Even if a recipe for a successful biosensor is impossible to determine a priori, a look at the biosensor market gives some hints on the common characteristics of today's commercially successful devices. The most cited example of a commercial biosensor is the glucose biosensor, which

represents a considerable fraction of the sales of biosensors worldwide.[19] In these devices, a drop of blood (1-50 µl) is needed in order to detect a sufficient number of glucose molecules (targets) within a few tens of seconds.[19] Another example of a biosensor that is readily available is the pregnancy test. In this device, the presence of the hormone human chorionic gonadotrophin (hCG) in urine is commonly detected by means of agglomeration of antibody-modified gold sol gel particles mediated by the hormone itself.[20] A filter discriminates between the agglomerated and non-agglomerated particles, thus turning the screen of the device visibly pink in presence of a sufficient quantity of hCG. The latter example is a peculiar example of an optical biosensor where the biological recognition is transduced into an optical contrast, i.e. a change in color detectable by the naked eye.

A large number of alternative biosensor platforms are also commercially available, but primarily used in clinical or research settings. This stems from the fact that they are relatively labor intensive and because the analysis requires trained personal. Examples include enzyme-linked immunosorbent assay (ELISA)[21] and the polymerase chain reaction (PCR).[22]

The success of the glucose sensor and the pregnancy test originates to a significant extent from a combination of i) a sensitivity that meets the need, ii) reliability, i.e. device delivering reproducible outcomes and iii) ease of large-scale manufacturing at affordable costs. However, both the glucose biosensor and the pregnancy test tackle situations in which the analyte is present at relatively high concentrations (in the mM to µM regime). Unfortunately, this is not the case for early diagnostics of most other diseases which are considerably influencing the lives of millions of patients per year, among those cancer,[23] myocardial infarction[24] and Alzheimer's disease.[25] Here, the biomarkers (targets) are often present at concentrations down to the pM regime or below, i.e. several orders of magnitude lower than in the previous examples. The accuracy required to detect such low concentrations essentially sets the required standard of a generically applicable biosensor.

To better understand the correlation between target concentration and surface coverage, a model describing the nature of the probe-target interaction is presented below. Under the assumption that the binding between the target and the probe is reversible, i.e. the target can be released from the probe after binding, two reaction coefficients, k_{on} and k_{off}, are used to describe respectively the binding and the release processes. The time dependence of the surface coverage Θ is given by the Langmuir isotherm model:

$$\frac{\partial \Theta}{\partial t} = k_{on} C(\Theta_{max} - \Theta) - k_{off}\Theta \tag{1}$$

where Θ_{max} is the surface coverage at saturation, i.e. when there are no more available binding sites and C is the concentration of the analyte.

The link between concentration and surface coverage can be further exemplified by evaluating eq. 1 at equilibrium, i.e. $lim_{t\to+\infty}$:

$$\Theta = \Theta_{max}\frac{1}{1+\frac{K_d}{C}} \tag{2}$$

where K_d is the equilibrium dissociation constant and is defined as the ratio between k_{off} and k_{on}. In this model, all the parameters related to the biorecognition event are completely described by just the affinity constant. Thus, by knowing the nature of the interaction, eq. 2 leads to a direct correlation between the concentration, C, and the surface coverage at equilibrium, Θ. Even in the case of strong affinity, for example an antibody-antigen interaction (K_d = 1 nM),[26] the surface coverage at equilibrium is already smaller than 1 % with respect to the maximum surface coverage, for concentrations in the order of 10 pmol. In essence, a low analyte concentration converts into a low equilibrium surface coverage, which in turn translates into signals that might be below the noise threshold. For this reason, there is a demand on sensors capable of detecting of a measurable response at as low surface coverage as possible, in other words sensors with high sensitivity.

This demand for improved sensitivity is tackled by tailoring the physical design of the sensor with respect to the desired biorecognition reaction. Common strategies include: i) optimizing the measurement: devices used for detection, treatment of the measured response, etc. ii) design of the actual sensor element by choosing the most suitable material, for example silver[27] or gold[28] elements in plasmonics; iii) implementation of strategies to minimize the background contribution to the signal, for example by localizing the sensitivity to within a few nanometers from the interface sensor-medium;[29–31] iv) modification of the surface properties of the detector element to maximize the signal, for example allowing the binding to high-sensitivity areas only.[32]

As mentioned above, the surface of the sensor has also to be functionalized in order to enable just the desired analyte to generate a signal, i.e. the sensor must provide high selectivity. This is typically ensured by anchoring bio-molecules acting as probes to the detector element while making the underlying surface inert for all other reactions.[17,32]

At the same time, even if both the sensitivity and the selectivity of a sensor are high enough to detect target molecules at concentrations being a fraction K_d of the interaction, see eq. 2, the response of the sensor must be obtained within a reasonable time scale. Therefore, the sample liquid has to be handled such that the target molecules are efficiently transported from the bulk

to the sensor surface. Improved transport conditions, without sacrificing high sensitivity, can in fact be achieved by miniaturizing the key components of a biosensor. One may thus envision that binding reactions at the interface of a nanoscale sensor could yield comparably larger contrasts in the physical properties utilized to convert the binding reaction into a detectable signal than that of sensors with larger dimensions, thereby reducing the number of target molecules per surface area, i.e. surface coverage required in order to generate a detectable signal. First, by reducing the dimension of the sensor element, samples volumes can be reduced by rescaling the liquid channels down to the micro- and nano dimensions.[33] Second, a combination of small-scale fluidics and nano-scale sensor elements may also enable more efficient transport of analyte molecules to the sensor element, as schematically shown in Figure 1 and articulated in the text box below. In essence, conditions can be reached in which it is rather the rate of the actual biorecognition reaction than the diffusion of the analyte molecules that determines the time response of the sensor.[34]

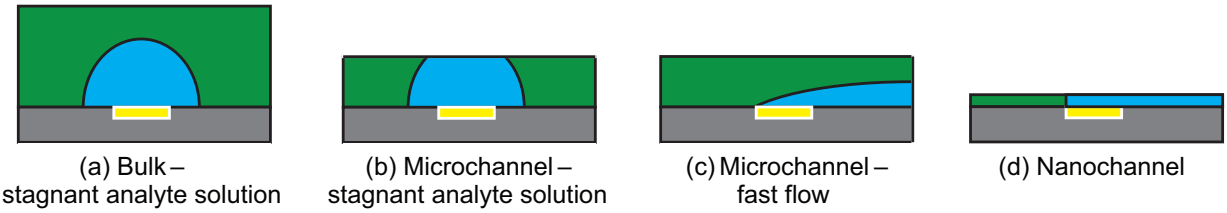

Figure 1: A schematic representation of different flow configurations (a-d). A depletion layer (light blue) is generated when targets from the analyte solution (green) bind to the probe molecules on the sensor surface (yellow). The presence, profile and extension of the depletion layer are determined by the geometrical constraint of the channel and by the applied flow.

Text box: influence of channel size and flow speed on analyte transport

The analyte solution (green in Figure 1) is in contact with the sensor surface (yellow). The binding of the targets to the probe molecules on the sensor generates a depletion layer (light blue) where no target molecules are present. The time response in mass-transport limited regime, depends on the rate of transport of targets to the sensor surface rather than on the kinetics of the biorecognition reaction. Considering a stagnant analyte solution, the transport is purely diffusive since it is determined by the concentration gradient between the analyte solution and the depletion layer. This translates in bulk, Figure 1(a), to a depletion zone which is infinitely growing in every direction, and therefore to non efficient transport. If the

sensor is integrated in a microfluidic network, the growth of the depletion layer will be suppressed by the height of the channel even in stagnant condition, Figure 1(b). Moreover, the transport rate and the profile of the depletion layer can be dramatically changed by applying a flow perpendicular to the sensor surface. For fast flow rates (above tens of $\mu m\, s^{-1}$*), Figure 1(c), the extension of the depletion layer in height is for protein molecules typically limited to approx. 10* µm*.[35] In this case, the target molecules must diffuse through a significantly smaller depletion zone to reach the sensor surface compared to case (a) and (b). Thus, the time response of such a sensor is considerably faster than in the case with a stagnant analyte solution. However, a fast flow leads also to increased sample consumption with respect to the stagnant cases even if the time to reach equilibrium surface coverage is shorter.[36] This is due to the high number of target molecules leaving the channel without having a chance to bind on the sensor surface due to lack of proximity to the depletion layer. This problem could be overcome by further reducing the size of the channel into the nanometer range, Figure 1(d). In this case, the size of the channel ensures that every target molecule transported through the channel is given a chance to diffuse to and bind at the sensor surface. This faster transport mechanism combined with high capture efficiency could potentially lead to exceptional performances of such system for detection of low-abundant analytes in small volumes, and constitutes a key motivation of this thesis work.*

The aim of this thesis work is to contribute to these goals using a combination of top-down and bottom-up nanofabrication schemes of sensor devices providing sufficiently simple liquid handling protocols and readout principles for efficient use outside advanced laboratory settings. Ease of sensor readout was accomplished by utilizing the exceptional optical properties of nano-scale noble metals particles. In fact, the optical properties of these nanoparticles are highly sensitive to changes in the refractive index at the interface between the structure and the surrounding medium. This enables label-free detection of biomolecular binding events in real-time by simply monitoring the far field optical properties, i.e. color, of an ensemble of nanoparticles. Small scale liquid handling was accomplished using a combination of microfluidics and nanofluidics, where the latter was accomplished by positioning nano-scale sensor elements within nano-scale pores that penetrate a 220 nm thin suspended silicon nitride membrane and the former - although still work in progress - was obtained by integrating these sensor elements with relatively conventional soft-lithography-based microfluidics.

In Chapter 2, I will present the basic physical principles behind nanoplasmonics with particular focus on its applicability to biosensing. Chapter 3 introduces the techniques necessary for the

development of the nanofabrication processes employed in this work. A summary of the contributions is presented in Chapter 4 along with an outlook on the future extension of this thesis.

2 Nanoplasmonics

This chapter introduces the basic physical principles behind nanoplasmonics. A description of a standard setup for tracking changes in nanoplasmonic signals is also presented along with a summary of the advantages of nanoplasmonics for label-free sensing applications.

2.1 Introduction to nanoplasmonics

The search for an in-depth understanding of the vivid colors of ”small” noble metal particles took off many centuries after their use for fine arts. Being an experimentalist myself, I would like to introduce the topic mentioning the pioneering work of Faraday, who in the mid-19th century systematically analyzed the dependence of the optical properties of noble metals on their physical properties.[37] He noticed that the color of gold particles and thin films varied throughout the visible spectrum in a systematic fashion depending on size, aggregation state and environmental conditions. Since then, it took about 50 years before the first publication providing a theoretical description of these phenomena was published in the early 1900's by Mie.[38]

Mie's work describes the interaction of light with spherical particles of arbitrary size in terms of light absorption and scattering, i.e. extinction, obtained by analytically solving the Maxwell's equations. These solutions are valid for the analysis of disperse particle systems in the electrostatic dipole regime at wavelengths significantly longer than the dimension of the particles. In particular, an ensemble made up of nanospheres, that are much smaller than the wavelength of light, enhances the extinction of light within a certain wavelength range. In the case of metal nanoparticles, the wavelength region at which resonance occurs is in the visible spectrum. As a consequence, the particles have a color recognizable by the human eye.

The strong extinction of light originates from its interaction with conduction electrons that, for specific wavelengths, are excited to oscillate collectively at a metal-dielectric interface, as schematically represented in Figure 2.[39]

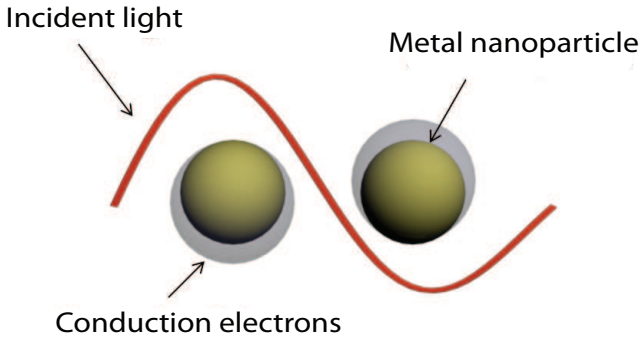

Figure 2: The incident light interacts with the conduction electrons of the metal nanoparticles. The electrons oscillate collectively in phase with the incoming wave.

This collective motion of free electrons is referred to as surface plasmons and the study of the interaction of light with metal nanostructures is referred to nanoplasmonics or localized surface plasmon resonance (LSPR).
The possibility to use nanoplasmonic structures for sensing derives from the dependence of their optical properties on the surrounding environment. In the following paragraphs, I will derive an explicit relationship connecting intrinsic optical properties of gold nanoparticles to local refractive index changes for the simplest possible case of interest, that is a disperse ensemble made up of nanospheres.
In this case, the optical cross-section of a non-dense system of nanospheres (much smaller than the wavelength of light), can be identified as:[38]

$$\sigma(\lambda) = \frac{18\pi V}{\lambda} n^3 \frac{\varepsilon_i(\lambda)}{(\varepsilon_r(\lambda) + 2n^2)^2 + \varepsilon_i(\lambda)^2} \tag{3}$$

where: V is the volume of the structure
λ is the wavelength of the radiation
n is the refractive index of the surrounding medium
ε_i is the imaginary part of the dielectric function of the metal
ε_r is the real part of the dielectric function of the metal

It is obvious that the resonant condition, i.e. the condition for the excitation of the localized surface plasmon, is fulfilled when the denominator of $\sigma(\lambda)$ goes to zero:

$$(\varepsilon_r(\lambda) + 2n^2)^2 + \varepsilon_i(\lambda)^2 = 0 \tag{4}$$

It is worth mentioning that for gold and silver nanoparticles, it is possible to assume a relatively small $\varepsilon_i(\lambda)$.[40] Thus, the resonance condition can be simplified to:

$$(\varepsilon_r(\lambda) + 2n^2) = 0 \tag{5}$$

At this stage, the equation linking λ and the refractive index n can be further simplified by substituting into eq. 5, the relation between ε_r and λ valid in the Drude model:[41]

$$\varepsilon_r(\lambda) = 1 - (\frac{\lambda}{\lambda_p})^2 \tag{6}$$

where λ_p is the plasma wavelength. Thus, eq. 5 becomes:

$$\lambda_{peak} \quad \alpha \quad \sqrt{2n^2 - 1} \tag{7}$$

This simple equation illustrates the foundation of nanoplasmonic sensing. In fact, the resonance peak, λ_{peak}, is directly related to the refractive index, n, of the medium surrounding the nanosphere. This means that any binding onto the nanosphere that will change locally the refractive index will be detectable in the far field by monitoring a shift of λ_{peak}.
At this stage, it is convenient to introduce a parameter which represents how the resonance peak responds to changes in refractive index, the bulk sensitivity S. Thus, the bulk sensitivity can be defined as the derivative of the resonance peak with respect to the refractive index:

$$S = \frac{\partial \lambda_p}{\partial n} \quad \alpha \quad \frac{4n}{\sqrt{2n^2 - 1}} \tag{8}$$

The bulk sensitivity S depends on the refractive index, but weaker if compared with λ_{peak}, eq. 7. In addition, the shifts of refractive index due to biomolecular binding events are usual of modest magnitude. For this reason, the induced change in sensitivity is negligible in most of the biosensing experiment and the sensitivity is generally approximated as constant.[42]
So far, the set of equations for spherical small nanoparticles were used to give a picture of the main variables involved in nanoplasmonics, being the size, the dielectric function and the sur-

rounding refractive index. However, recent advances in nanotechnology allows for fabrication of much more complex shapes, for example nanorods,[43] nanorings,[44,45] and nanocrescents.[46,47] The development of this complexity in size and shapes was driven not only by the will of increasing the understanding of the physical principles, but also by the intense search for the optimal shape in sensing applications. While the main concepts presented in the simple case described above are still valid, the description gets mathematically more elaborate. However, in some cases, qualitative predictions of the resonance of complex structures can be obtained by just introducing a shape factor χ into eq. 5:

$$(\varepsilon_r(\lambda) + \chi n^2) = 0 \tag{9}$$

The shape factor χ varies with spatial conformations and contains all the shape related information. Briefly, χ is 2 for a sphere and increases with the aspect ratio of the nanoparticle.
Several models and simulation tools have been developed to further improve quantitative predictions of complex shapes. The two most widely used are based on brute-force computational solution of Maxwell's equations namely, finite-difference time domain (FDTD)[48] and discrete dipole approximation (DDA).[49] These simulations tools provide detailed far and near field predictions at the price of computational time and model complexity. Worth mentioning is also the more intuitive approach introduced with the plasmon hybridization theory which decomposes complex structures in simple elemental shapes that interact with each other.[50]

2.2 Probing nanoplasmonics

As mentioned previously in this chapter, nanostructures extensively scatter and absorb light when their plasmonic mode is excited. While the human eye is sensitive enough to detect effects of artistic relevance, the resolution needed for sensing requires in most cases more sophisticated electronic devices.
A schematic of a setup designed to probe extinction caused by an LSPR-active substrate is shown in Figure 3.

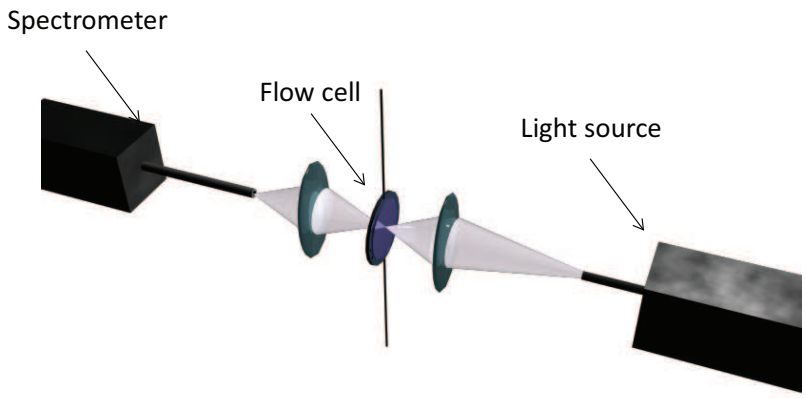

Figure 3: Schematic illustration of an extinction LSPR setup. The light is focused on the flow cell by a lens and collected by a spectrometer.

The minimum set of components needed in a typical setup for monitoring nanoplasmonics consists of a light source, a measurement cell and a detector. The light source and the detector ensure changes in the transmitted light to be transduced into a detectable output and the measurement cell permits the exposure of the sample to a controllable atmosphere.
Briefly, in the setup used in this work, white light is generated using a tungsten-halogen source and coupled to an optical fiber. A lens then focuses it on the sample where it interacts with the nanoplasmonic structures. In this setup, the probed area is mainly determined by the fiber diameter;[51] but it can be reduced to less than hundreds of μm^2 by using a microscope.[51] Afterwards, the transmitted light is collected through a lens and coupled into a detector, a spectrometer in most of the cases. In this configuration, the light transmitted through the flow cell will interfere with the nanostructures and lose intensity due to scattering and absorption at the wavelengths at which the plasmonic resonance occurs. Therefore by detecting the transmitted light, it is possible to monitor the shift of the plasmonic peak induced by local refractive index changes caused by, e.g. biomolecular binding events.
In order to isolate the contribution to the signal from the plasmonic nanostructure, a reference is usually acquired and used in the evaluation of the optical extinction, $E(\lambda)$, caused by the structure. Thus, the amount of light that is prohibited to be transmitted due to the plasmonic response

is obtained from:

$$E(\lambda) = -log\frac{I_{sample}(\lambda)}{I_{reference}(\lambda)} \tag{10}$$

An illustration of a shift in the extinction spectrum caused by a biomolecular binding event is shown in Figure 4. Upon a change in refractive index, the blue spectrum recorded before the event turns into the red one. Since the entire spectrum red shifts, multiple parameters can be used to analyze a binding reaction: the shift of the peak or of its centroid,[52] or the magnitude of the extinction at a specific wavelength can be used to analyze a binding reaction. The latter approach has the advantage of excluding the need of a spectro-photometer as detector. In this case, a simple light emitting diode (LED) and a photosensitive p-n junction is enough to detect the biorecognition reaction, as we show in paper I.

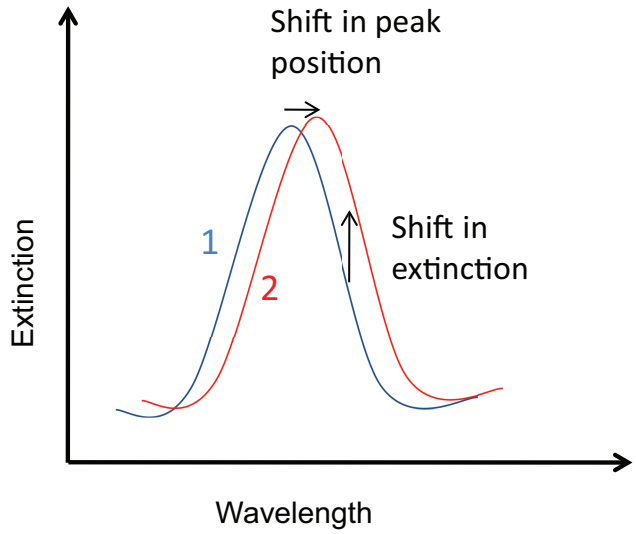

Figure 4: The graph illustrate how a redshift (1-2) of the extinction peak results in both a change in peak position and a change in the extinction at a given wavelength.

2.3 Nanoplasmonics for sensing

The physical principles behind nanoplasmonics open up for biosensing applications. To start with, the nanoplasmonic field generated at the interface between the metal nanoparticle and the dielectric medium is localized to the nanostructure with a decay length in the order of tens of nanometers for gold.[53] This localization of the field to the nanoscale implies that the nanostructures are responding to events in proximity of their surface only, and not to the same extent to changes in the bulk. The low sensitivity to changes in bulk leads to a simplification of the sensing setup, for example temperature control can be excluded.

The experimental setup can be further simplified compared with setup based on different optical transducer principles, for example surface plasmon resonance[54] (SPR) and waveguide spectroscopy.[55] This is so because measurements based on nanoplasmonic resonance do not put any demand on the coupling of light,[56] for example angle of incidence. Thus, the number and complexity of optical components in such setups could be significantly reduced, keeping in mind only eventual specifics on signal-to-noise and probed area. The combination of non-stringent requirements of the experimental setup and the small size of the particles have resulted in a recent explosion of miniaturized sensor concepts based on nanoplasmonics.[39]

The potential for miniaturization implies that the sensor is also well suited to exploit all the advantages deriving from nanofluidics. As described previously, an efficient transport of molecules to the sensor surface plays an important role in the detection of low-abundant analytes. In this framework, we explored in Paper II the possibilities of integrating nanoplasmonic particles onto the inner wall of nanochannels in a parallel network.

However, the miniaturization of the sensor element in nanometer-sized objects leads also to challenges regarding the uniformity of the sensitivity with respect to other surface-based sensors exploiting larger planar sensing surfaces, for example SPR[54] and quartz crystal microbalance (QCM).[13] While in the latter cases the sensitivity is homogeneous over the entire substrate, in the case of nanosized sensors, it is only the binding occurring onto the sensor surface which generates a signal. This is so because the sensing field decays within tens of nanometers from the interface between the nanoparticle and the surrounding medium.[53] Hence, material specific chemistries are needed to enable binding only on the sensitive components of the device while at the same time inhibiting reactions to occur onto the remaining areas using passivating films. The material contrast between the noble metal nanosensors, for example gold and silver, and the substrate, for example silicon nitride, silicon oxide and titanium dioxide, allows for orthogonal surface chemistry schemes to be adoptable for these purposes.[27,31]

In conclusion, nanoplasmonic biosensors have the potential to effectively tackle a broad variety of sensing challenges. On the one hand, the simplicity of the experimental setup and the potential for miniaturization is an important asset in the development of cheap and portable commercial biosensor for point-of-care diagnostic. On the other hand, the integration of a sensor into nanofluidic networks combined with material specific surface modifications preserving high selectivity could play a vital role in the search for concepts capable of detecting low-abundant analytes.

3 Nanofabrication as a toolbox

The behavior of materials changes dramatically at the nanoscale. Nature presents plenty of examples were nanoscale modifications of surfaces lead to extraordinary material properties. Take as an example the capability of geckos to adhere to a wide range of surfaces in arbitrary orientations. This enhanced attachment force is ensured by hundreds of projections presented on their feet. These projections terminate in 200-500nm spatula-shaped structures which allow them to efficiently exploit capillary and van der Walls forces.[57] Another popular example is the lotus flower. In fact, the leaves of lotus flowers are efficiently self-cleaning thanks to their ability to spontaneously form water droplets that move in response to gravity at their interfaces. The nanostructures that are naturally present on those surfaces yield a high contact angle for water which in turn ensures a very low roll-off angle.[58]
Nanofabrication gives mankind a toolbox to recreate these extraordinary material properties already present in nature, e.g. by creating a gecko-inspired tape,[59] or even entirely new materials or metamaterials, e.g. superhydrophobic structures[18] or materials with negative refractive index.[60] In this chapter, the toolbox of nanofabrication techniques used throughout this thesis is presented. For simplicity, the chapter is divided in two main sections with focus on characterization and fabrication techniques, respectively. An introduction paragraph puts emphasis on the advantages and disadvantages of the main techniques and their use in the presented work. The techniques are afterwards described in separate sections.

3.1 Characterization at the nanoscale

In this section, the main characterization techniques used in this thesis are presented. Scanning electron microscope (SEM) was the instrument of choice for imaging at resolutions well below the diffraction limit of light. This versatile instrument was used to resolve nanostructures, e.g. gold nanodisks (Paper I) or nanopores (Paper II). SEM also provided efficient feedback on the success of separate fabrication steps used throughout the processes. The reason for this is due to a suitable combination of imaging resolution in the nm range, simple sample preparation, imaging in few seconds and depth of focus in the order of hundreds of µm.
Atomic force microscope (AFM) was exploited for imaging at higher resolutions with respect to SEM and to get information about material properties, e.g. surface roughness, at the nanoscale. This technique provides three dimensional information of an interface without requiring advanced sample preparations or low pressure environment. However, the imaging area is restricted to tens of micrometers and the image acquisition is slow; several minutes are required per image.

Furthermore, due to the nature of AFM, a careful image analysis is required in order to extrapolate relevant data.
Ellipsometry was mainly exploited to obtain thickness and optical properties of dielectric films, e.g. silicon nitride membranes (Paper II). This technique allows for quick data acquisition over large areas, up to several inches, and relatively easy data analysis for homogeneous single dielectric layers.

3.1.1 Scanning electron microscope (SEM)

SEM is broadly employed for imaging of features in a dynamic range going from hundreds of µm to a few nm. A schematic illustration of the working principle of SEM is shown in Figure 5.

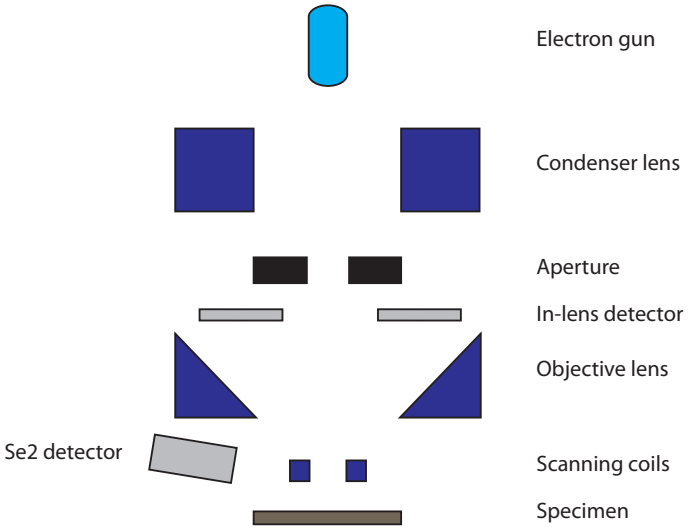

Figure 5

Briefly, an electron beam is generated either by thermionic emission (tungsten and lanthanum hexaboride tips) or by field emission (sharp tungsten tip) at the electron gun. The generated beam is accelerated at a specific acceleration voltage applied between the electron gun and the specimen and focused using a first stage of condenser lenses. A trade-off between high probe current, which is linked to high contrast, and small beam size, which is linked to high resolution, is determined by the dimensions of the circular aperture located after the condenser lenses, ranging from 7,5 µm to 120 µm in diameter. Objective lenses focus the beam onto the sample and scanning coils are used to deflect the beam in order to enable scanning over a selected area.
The electron beam interacts with the specimen and generates secondary products according to its energy and penetration depth. The inelastic scattering of the incoming electrons with the atomic

core or shell of the specimen's atoms in an interaction volume of a few nanometers from the surface generates secondary electrons (SE). The elastic scattering with atoms located in much deeper regions of the sample generates backscattered electrons (BSE). The first category of electrons, SE, carries information about the topography of the sample due to the interaction volume being limited to within few nm. The latter category, BSE, conveys information on the material properties of the sample being dependent on the atomic number of the interacting atom. Dedicated detectors acquire the different electronic signals and allow for image generation on a monitor.

Two different types of detectors were available for detection of SE in the instrument used in this thesis, namely the SE2 detector and the In-lens detector. These two detectors are placed at different locations in the instrument. The SE2 detector is placed just outside the column that guides the electron beam, while the In-lens detector is placed in the electron beam path. Such placement allows the In-lens detector to be used at lower voltages, allowing it to collect signals from electrons generated at a smaller penetration depth compared with the SE2 detector. This leads to a smaller focus depth but higher resolution of surface properties for the In-lens detector compared with the SE2 detector, see Figure 6, while in contrast higher topographic contrasts can be obtained using the SE2 detector, operated at higher voltages.

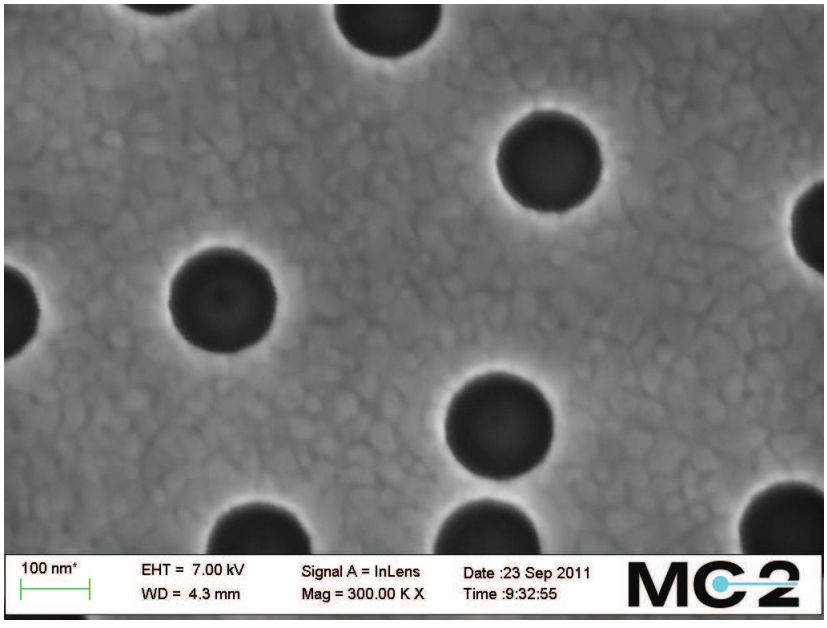

Figure 6: Micrograph of nanoholes in a gold film acquired with the InLens detector. The grain size of the gold film is visible while the depth of the hole is not clearly recognizable due to flattening of the image.

3.1.2 Atomic force microscope (AFM)

The atomic force microscope (AFM) is a valuable microscopy tool for high resolution imaging and local acquisition of material properties at the nanoscale. In this setup, a sharp probe scans the sample surface, thus monitoring the intermolecular and surface forces between the sample and the probe. The nature of the interaction allows measurements in the sub-nanometer range on any type of specimen, also in liquid environment.[61] A simplified schematic of a typical AFM is shown in Figure 7.

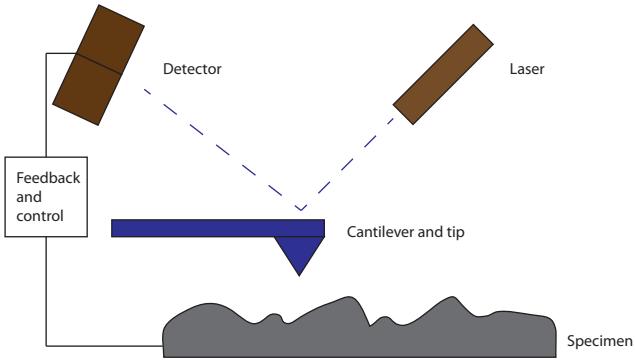

Figure 7: Simplified schematic of an AFM setup.

A sharp tip is located onto a soft cantilever which is controlled to move with high precision in the plane of the specimen. The deflections of the cantilever due to the interaction forces with the specimen are monitored by a laser-detector system. A laser beam is shone on the back side of the cantilever and the reflection is monitored by a four-quadrant photodiode detector. The variation in the position/oscillation of the cantilever along the axis perpendicular to the sample surface is tracked by the change in the position of the reflected laser beam onto the detector.
Different working modes can be used, depending on the nature of the interaction between the tip and the substrate: dynamic, such as non-contact mode and tapping mode; and static, such as constant-force contact mode and constant-height contact mode. The difference between the static and the dynamic modes is defined based on contact or lack of contact with the sample. In static modes, the cantilever is always in contact with the substrate. Thus, the topography of the surface is acquired by measurements of the deflection of the cantilever. In dynamic modes, the cantilever oscillates near its resonance frequency, intermittently contacting the surface of the sample in tapping mode. In both non-contact and tapping mode the variations in amplitude, phase and frequency of the oscillations are recorded in order to map the surface of the sample.

3.1.3 Ellipsometry

Ellipsometry is based on measuring the change in state of polarization of polarized light beams reflected at an interface. Reflection of plane-polarized light at an interface leads to changes in both the amplitude and the phase of the incoming electromagnetic wave. For incident plane-polarized light, the reflected light will become elliptically polarized and attenuated. The magnitude of changes in phase and amplitude depends on wavelength, the angle of incidence, the film thickness and its refractive index. A typical ellipsometry setup is proposed in Figure 8.

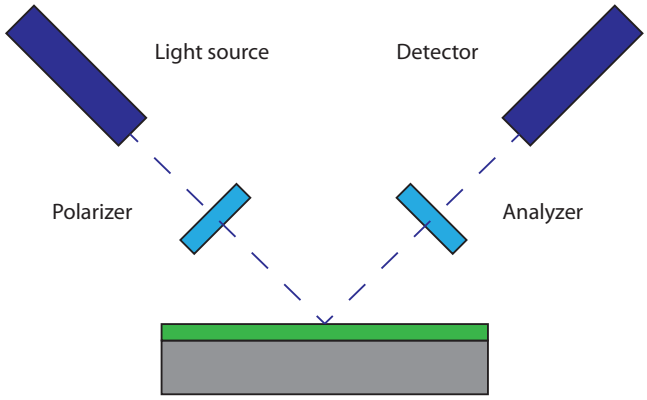

Figure 8: Schematic representation of a simple ellipsometry setup.

The light source is linearly polarized and shone on the sample. The reflected light is transmitted through a second polarizer, called analyzer, and detected by a photodetector. By measuring at known wavelengths and angles, film thickness and index of refraction can be determined with high precision. In order to further improve the quality of the measurement, multiple independent measurements can be made by varying angle and wavelengths of the incoming light beam.

3.2 Fabrication at the nanoscale

In this section, a brief overview of the main techniques used for the nanofabrication of nanoplasmonic sensor substrates is presented. Two main moments of a fabrication process can be identified, such as pattern transfer and deposition of thin films. The patterning methods can be grouped into two main categories, such as lithography and etching techniques. While the first category comprises processes forming patterns on the surface of a substrate, the latter comprises the ones transferring it into the underlying layer by removal of material, i.e. etching. Many lithographic patterning methods have been developed in the recent years differing from each other because

of the different mean used to transfer the pattern, for example light (*phos-* in greek) in photolithography or electrons in electron beam lithography. The two lithographic methods used throughout this work were photolithography and colloidal lithography. These techniques were chosen keeping in mind the possibility to develop process with high potential for translation to industrial contexts. In fact, both photolithography and colloidal lithography enable patterning large areas, up to several inches, while simultaneously preserving the possibility to fabricate devices in a fast, cheap and scalable manner. Photolithography was used to pattern in the millimeter to micrometer range, e.g. to define the outer dimensions of the chips and silicon nitride membranes used as a sensor element in Paper I and II, while colloidal lithography was used for the nanoscale fabrication, e.g. plasmonic nanodisks (Paper I) and nanopores (Paper II). Colloidal lithography was chosen instead of electron beam lithography, which is today considered the most established nanofabrication method, because self-organization of colloidal nanoparticles allows for faster and less-expensive processing. In fact, colloidal lithography enables the fabrication of nanostructures on large regions, up to several inches, without losing control on dimensions and distribution. The main limitation, however, concerns the limited choice of geometries[56] in comparison with more flexible techniques like electron beam lithography[62] and focused ion beam lithography.[63]

After pattern definition, a combination of dry etching processes, such as ion milling and reactive ion etching (RIE), and wet etching processes was used to transfer the pattern into the substrate. This combination allows for fine tuning process parameters with respect to the desired need. The main etching parameters are: etching speed, i.e. how fast the material is removed; material selectivity, i.e. how the etching speed varies depending on the etched material; and etch rate anisotropy, i.e. how directional is the etch, where a high anisotropy corresponds to a high directionality. Ion milling was primarily employed to achieve anisotropic etches, without material specificity, for example shaping of the gold nanosensors (Paper II). RIE was the choice for anisotropic etches with good material selectivity, for example nanopatterning of photoresist (Paper I) and fabrication of nanopores (Paper II). Wet etching was mainly used thanks to high selectivity and speed, for example removal of the silicon underneath the silicon nitride membranes (Paper II).

Fabrication at the nanoscale also requires design processes which can transfer atoms onto the substrate, in other words growth of thin films. The wide range of existing thin-film deposition processes can be categorized according to the underlying physical principle being utilized. In this work, physical vapor deposition (PVD), mainly electron-beam assisted evaporation, was used for deposition of metallic films, while chemical vapor deposition (CVD), mainly plasma enhanced

CVD and low pressure CVD, was used for dielectric films. In PVD, thermal energy is transferred to atoms, for example by means of an electron beam, which in turn evaporate or sublimate from the source. This vapor then diffuses and deposits onto a substrate, thus creating a thin film in a controllable manner. In CVD processes, a compound in gaseous phase reacts with other gases inserted in a chamber, leading to a chemical reaction, the solid product of which becomes deposited on a substrate. PVD was chosen because of its directionality, cleanliness and flexibility in the choice of materials, for example deposition of gold nanodisks (Paper I) and of chromium masks and gold nanosensors (Paper II). CVD was employed for growth of high quality dielectrics with low stress, few defects and with good step coverage, for example silicon nitride coatings for insulation (Paper I) and silicon nitride membranes (Paper II).

3.2.1 Photolithography

Photolithography is a process to pattern substrates over large areas, being widely used both in industrial and academic settings. The working principle is illustrated in Figure 9.

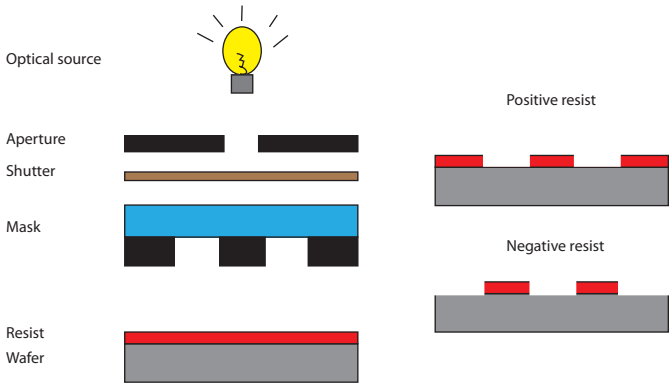

Figure 9: Schematic of a basic photolithography process.

An optical light source is used to expose a wafer coated with a photosensitive material, i.e. a photoresist. The length of the exposure is determined by a shutter and the area exposed is determined by a mask. The mask is usually a highly polished optical transparent glass coated with a patterned opaque layer, typically chromium. The light shone through the non-opaque areas of the mask reaches the resist and activates chemical (resist specific) reactions in the polymer. In the case of positive photoresists, the exposed areas dissolve faster than the unexposed ones, leading to a pattern which resembles the one present on the mask. The response of negative resists is the opposite, i.e. the exposed areas are more resistant than the unexposed ones.

The size of the patterned area can easily reach 6 inch. The resolution is determined by a combination of wavelength of the optical source, usually in the UV range, and quality of the mask, determined by the resolution of the pattern and pin hole density. The precision in the alignment of the pattern to preexisting features on the substrate is mainly determined by the quality of the mask aligner, i.e. precision of the stage movement and of the optics. Resolution reaching on the order of 100 nm can be achieved with common resists under optimal conditions.[64] However, in conventional settings, photolithography is used for features down to around 1 µm.

3.2.2 Colloidal lithography and Hole-mask Colloidal lithography (HCL)

Colloidal lithography exploits the self-assemble of nanometer-size colloids on a surface to define masks for nanopatterning of substrates. Negatively charged polystyrene colloids are first dispersed in a solution which is exposed to the surface to be patterned. The negatively charged beads absorb electrostatically on positively charged surfaces. For this reason, a monolayer of positively charged electrolyte (Aluminum Chlorohydrate or Polydiallyldimethylammonium chloride) is adsorbed onto the surface prior to exposure to the colloidal suspension. Electrostatic repulsion forces between the negatively charge polystyrene colloids determines the average distance between the adsorbed particles.[56] This distance can be controlled by varying the concentration of screening charges in the solution, i.e. by increasing or decreasing the salt concentration. After saturated binding, the substrate, which can have macroscopic dimensions, becomes patterned with a monolayer of randomly adsorbed nanometer-sized polystyrene colloids displaying a short-range order determined by the distance between the nearest neighbors.
This monolayer can be used as an evaporation mask for transfer of the pattern into a metal film. Fter metal evaporation, a continuous metallic thin film with short-range ordered nanoholes is obtained by lift-off of the colloids, by e.g. tape stripping. The shape of the nanoholes is defined by the angle of evaporation, as shown in Figure 10. However, the thickness of the metal film is limited by the size of the colloids since films thicker than the radius of the beads will lead to a difficult lift-off process. This metal film can be used as a mask itself, e.g. for milling of nanopores in the suspended membrane presented in Paper II.

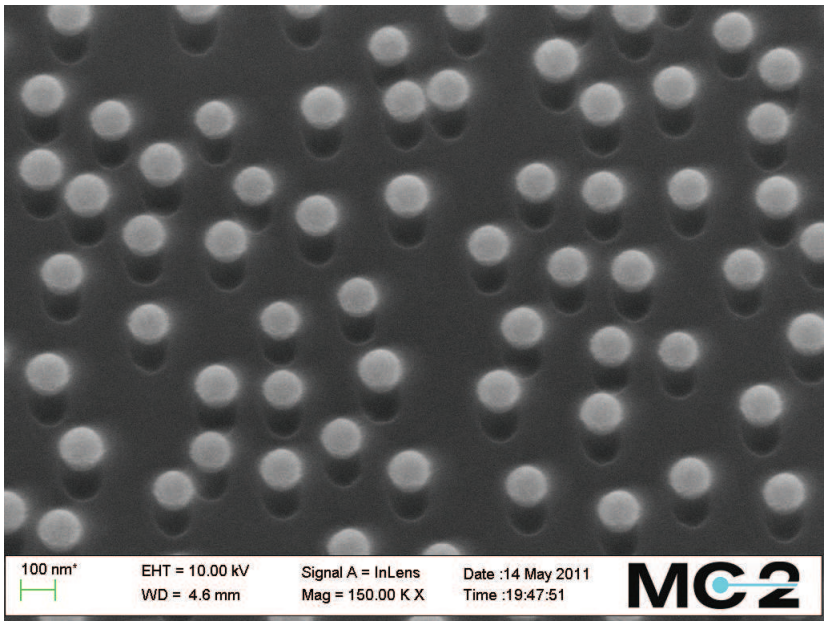

Figure 10: Micrograph of a thin film of chromium evaporated onto a monolayer of colloids. Elliptical nanoholes are created thanks to the shadowing provided by the colloids.

Colloidal lithography is also useful not only in order to fabricate porous films, but also for fabrication of discrete nanoscale structures. In particular, the metal nanodisks presented in Paper I were all fabricated by Hole-Mask Colloidal Lithography (HCL).[65] A brief summary of the main steps involved in the process adopted for the fabrication of gold nanodisks is presented in Fig. 11.

In brief, a thin layer of around 100 nm of polymethyl methacrylate (PMMA) positive resist is first deposited on the substrate [Fig. 11b]. This layer will act as a sacrificial layer for the fabrication of discrete disks on the substrate. As in colloidal lithography, the surface is then modified with an electrolyte (Aluminum Chlorohydrate) in order to improve the adhesion of the colloids to the substrate [Fig. 11c].

A metal mask is then deposited [Fig. 11d] and patterned by removal of the short-range ordered colloidal particles by tape-stripping [Fig. 11e]. As described above, a metal mask with a uniform distribution of short-range ordered nanoholes is thus created. Subsequently, the parts of PMMA not covered with a metal mask are removed through plasma ashing [Fig. 11f], allowing for deposition of material, e.g. gold, directly onto the substrate [Fig. 11g]. Gold nanodisks are thereby created and the remaining material removed through lift-off [Fig. 11h] of the PMMA. This results in a short-range ordered distribution of gold nanodisks onto the substrate.

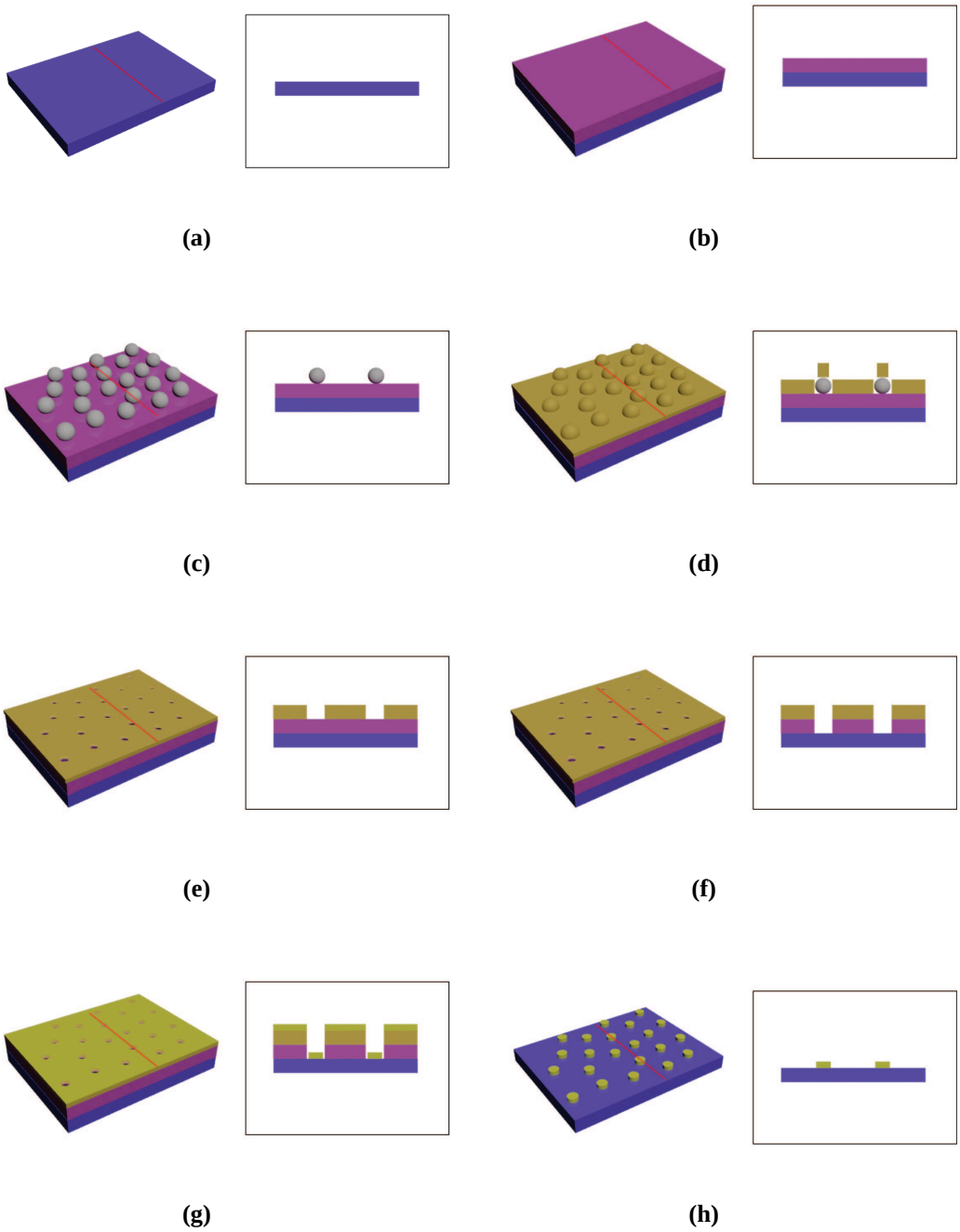

Figure 11: Schematic procedure of hole-mask colloidal lithography.

3.2.3 Ion milling

Ion milling is a purely mechanical process where heavy ions collide at high energy onto the substrate causing mechanical damage. Argon gas is preferably employed thanks to the inert nature of noble gasses, which guarantees a purely mechanical etch, and the high atomic weight. The most common configuration for ion milling sources is the Kauffman source. A schematic of such a source and the working principle of the process are presented in Figure 12.

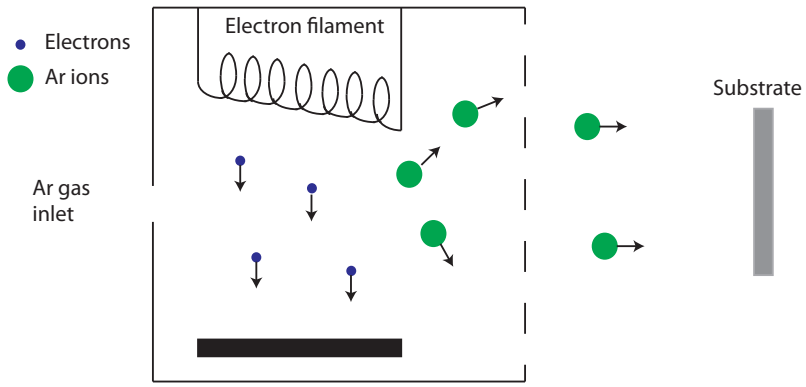

Figure 12: Schematics of a Kauffman source integrated in an ion milling process.

Electrons are generated by a heated filament and accelerated towards an anode by a constant potential difference. These high energy electrons travel through the chamber and ionize the Argon molecules injected in the system. The newly generated Argon ions are directed at high energy towards the substrate by a potential difference between the cage of the source and the substrate holder. Variation of parameters like gas flux and potential difference between the cage and the holder determines ion flux and impact energy. This leads to a process characterized by a high directionality of the etching with no chemical reactions at the specimen. However, the material selectivity is typically low; therefore thin resists or long etching times are typically not suitable for this process.

3.2.4 Reactive Ion Etching (RIE)

RIE is a combination of physical and chemical etching, where the latter plays a fundamental role in reaching high material selectivity. Briefly, a gas, called precursor gas, is exposed to low-pressure plasma in order to generate chemical species capable of reacting with the substrate. These reactive species diffuse to the surface of the substrate and adsorb. Chemical reactions occur at this interface and by-products containing substrate atoms are generated. These new chemical

compound are volatile and desorb from the surface, being pumped out from the chamber. The etching rate for this process is typically quite low because of the interfacial nature of the chemical reactions. For this reason, heavy ions are produced in the chamber and accelerated towards the substrate to increase the desorption rate, as in ion milling. However, the ion flux is low enough to not cause substantial physical damage to the substrate. Typically, fluorinated gasses, e.g. CF_4 and NF_3, are used for etching of silicon nitrides and oxides; while chlorine gasses, e.g. Cl_2, are particularly effective for etching of silicon.

3.2.5 Wet etching

Wet etching is at the opposite extreme in comparison with ion milling with respect to etching speed and material selectivity. In this process, the etching is purely chemical. The substrate is immersed in an etchant solution containing reactive species. The etchant species diffuse to the surface of the wafer and create soluble by-products at the interface. The by-products are transported away from the substrate to allow fresh etchant to reach the interface. The pure chemical nature of this process guarantees high material selectivity, however the uniformity of the etch rate depends heavily on the mechanisms used for transport of the etchant species and by-products to and from the surface. In fact, the etching process usually produces gas bubbles at the film-etchant interface, and efficient removal of these bubbles is necessary to allow for fresh etchant solution to reach the substrate. For this reason, the etchant solution is often constantly agitated or continuously supplied to the substrate by for example spraying it directly onto it. The dependence of the etch rate on the removal of the waste hinders etching narrow features smaller than 2 µm due to the difficulties in transporting fresh etchant to such an interface.

3.2.6 Electron beam assisted evaporation

Evaporation is a PVD technique which has been extensively used in the last decades for deposition of metals. A schematic of a simple electron beam assisted evaporator is shown in Figure 13.

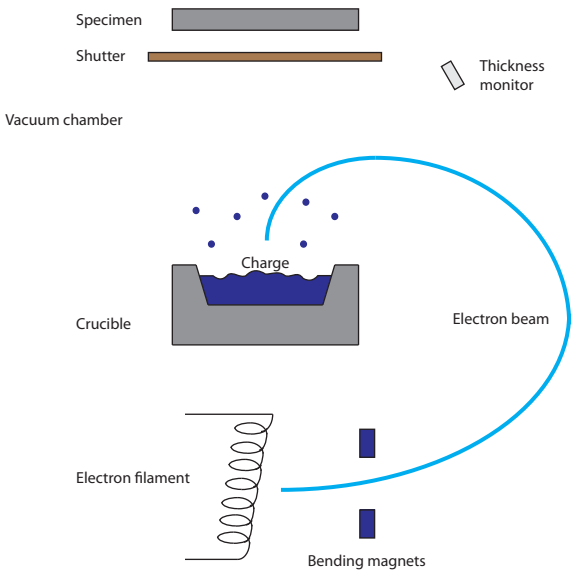

Figure 13: Schematics of a simple electron beam assisted evaporator.

Both substrate and the material to be deposited, called charge, are loaded into a vacuum chamber which is pumped down to low pressure. The charge is placed in a crucible, i.e. a container able to withstand high temperatures, and is heated by an electron beam. The electron-beam source is usually located beneath the crucible. The produced high-energy beam is tilted by a magnetic field to be directed against the charge. In order to melt uniformly the charge, the electron beam is scanned across the charge. Above certain material-specific temperatures, the molten charge releases vapor containing atoms which travel in a straight line through the chamber. That is because the mean free path of the atoms is much longer than the physical dimensions of the vacuum chamber thanks to a pressure in the range of 10^{-7} torr. Once a shutter between the charge and the substrate opens, these released atoms will deposit on the substrate and create a thin film. The thickness of the film can be monitored using a thickness monitor, usually a quartz crystal microbalance, placed in the chamber. The relation between the deposition rate on the substrate and on the balance depends mainly on their positions with respect to the source. It is worth notice that the thickness of the deposited layer will also depend on the orientation of the wafer and therefore on its geometrical dimension of it. The deposition obtained by electron-beam assisted evaporation is characterized by high directionality and poor step coverage. The main advantages of using an electron beam as a heating element are the fact that the charge is heated directly, allowing the crucible to be kept cold, and the minimal contamination deriving

from the source thanks to its positioning beneath the crucible.

3.2.7 Low pressure chemical vapor deposition (LPCVD) and Plasma enhanced chemical vapor deposition (PECVD)

These two deposition methods are variants of CVD processes. In contrast to PVD processes, CVD processes are purely based on chemical reactions. Typically, chemicals in gaseous form, called precursors, are fed into a chamber where the substrate is placed. These gases react in proximity to the substrate generating a set of chemical products. In heterogeneous processes, the products will undergo a set of subsequent reactions at the surface of the substrate only, thus leading to deposition of the selected material. Finally, the by-products are flushed out from the chamber. The deposited films, mostly dielectrics, are characterized by a conformal coverage of the substrate, which makes CVD popular for deposition of insulator materials.
There are numerous systems utilizing CVD principles, characterized by different pressures and temperatures used in the process. Throughout the thesis, two CVD systems were widely used, namely LPCVD and PECVD. In LPCVD processes, the energy for the activation of the chemical reactions is supplied by a high process temperature, typically above 500 °C, and the deposition of dielectrics occurs at low pressure, typically in the 0.1 torr range. Keeping the substrate at a high temperature leads also to a longer diffusion length for the compounds adsorbed at the interface. A long diffusion length translates into a higher chance for the adsorbed species to find a vacancy prior to bonding. For this reason, film uniformity is also improved by processing at high temperatures. However, some applications require the deposition to undergo at low temperatures to avoid damaging of the substrate. For this purposes, PECVD processes are preferred over the other CVD ones. In such systems, the energy is supplied by non-thermal sources like radio frequency (RF) plasma and the process temperature can be lowered to 300 °C instead than 700-1000 °C for deposition of nitrides. The drawback of this technique resides in the generation of films with poorer stoichiometry and density with respect to the ones generated by LPCVD processes. This difference in chemical quality of the films translates into a higher etch rate for the PECVD films, quality which has been used to selectively remove the protective PECVD silicon nitride layer while preserving the LPCVD silicon nitride constituting the membrane in Paper II.
Summarizing, in this thesis, LPCVD and PECVD were mainly used for growth of silicon nitride films. LPCVD was used when stoichiometry, uniformity and minimal internal stress were crucial, e.g. silicon nitride suspended membranes (Paper II). PECVD was preferred for low temperatures applications, insulation of chips (Paper I) or poor stoichiometry films, e.g. protection layer for the processing of the membranes (Paper II)

4 Summary and outlook

4.1 Summary of Papers

Paper I explores the possibility of combining LSPR based sensors and photodiodes for a novel biosensor with integrated detection. A typical nanoplasmonic biosensor setup consists of three separate components: a white light source, a sensor embedded in a flow cell and a spectrometer used to detect color changes induced upon biomolecular binding events at the sensor element. In this work, a high-intensity commercial LED was used as a light source, while the sensor chips had four integrated photosensitive regions as detectors. Gold nanoplasmonic structures were fabricated directly onto the photodiodes, thus integrating the sensor and the detector into the same chip. The nanoplasmonic structures were characterized and optimized for sensing. Shifts in light extinction at a single wavelength induced upon biorecognition events were transduced into electrical signals by the creation of electron-hole pairs in the detector. The generated photocurrent was acquired and tracked in real-time. The sensor was tested by detection of specific protein binding in a custom made flow cell.

Paper II presents the fabrication of a sensor chip designed to tackle the challenge of detection of analytes present at low concentrations in small volumes. For this purpose, a high-throughput fabrication process was developed for integration of gold nanoplasmonic structures in a nanofluidic network. A parallel network of nanofluidic pores was created into a thin silicon nitride membrane. Nanoplasmonic particles of different dimension and shape were fabricated simultaneously onto the inner surface of each pore. Their plasmonic resonances were proved to be tunable in the visible range by varying a single process parameter, and matched such that the overlap with the interference pattern of the silicon nitride membrane was minimized. The plasmonic properties of the nanoparticles were optimized for optical sensing, demonstrating a bulk sensitivity similar to that of conventional nanoplasmonic sensors.

4.2 Conclusions and outlook

There is an increasing interest in the development of novel biosensors in the foreseeable future. The impact on society of diseases connected to the aging of population, for example infectious diseases, cancer and Alzheimer's disease, has the potential of increasing the running costs of welfare over a sustainable threshold within few years. Early diagnostics and point-of-care testing will play a fundamental role in achieving a cost-effective health-care capable to satisfy the increasing needs. This translates into a drive towards further improved diagnostic devices where

miniaturization and enhanced performances enabling detection of low-abundant biomarkers is expected a key component. It is in this framework that engineering and science at the nanoscale could help delivering a new wave of cheaper, smaller, faster and better performing devices.
In this thesis work, the aim has been to translate advanced nanotechnology fabrication processes to novel biosensors platforms. The combination of novel nanofabrication schemes and nano transducer principles, i.e. nanoplasmonics, was exploited for challenging the performance of state-of-the-art sensors. The integration of sensor and detector elements onto the same chip resulted into a small and cheap biosensor with potential for the development into hand-held instruments (Paper I). The precise localization of the transducer element to the nanoscale enables the integration with nanofluidic schemes, which could play an important role in the detection of low-abundant analytes. A novel fully parallel nanofabrication protocol was developed for a scalable, reproducible and reliable production of such chips. A first benchmarking of the performances of such a sensor was carried out leading to comparable performances with current devices using the same transducer principle, but less efficient liquid handling.
Future work will focus on continuing the exploration of the potential of nanoscience in biosensing applications, aiming for either cheaper, smaller, faster and / or better performing biosensors. It is in this context important to keep in mind that certain challenges, e.g. the detection of minute concentration differences of low-abundant biomolecules in complex body fluids, are so demanding that also technically advanced and thus expensive solutions might turn out useful, while other challenges, such as translation of diagnostics from clinical settings to point-of-care diagnostics, put higher demands on low cost and high throughput. It is therefore of importance to early on in the process identify the actual application one bears in mind. In the first paper, the aim was clear: we aimed for a simpler and cheaper device. In the second paper, we were attracted by the potential advantage of directing the molecules to be detected through a fluidic channel with a dimension only an order of magnitude or so larger than the biomolecular targets itself and similar to the actual sensor element. However, the added value remains to be proven, and to do so, several steps remains to be taken and carefully analyzed. First, the nanofluidic chips presented in Paper II will be integrated with a fully functional microfluidic network for coupling the nanochannels to external liquid reservoirs. Second, material specific chemistry schemes, exploiting the material contrast between the silicon nitride nanochannels and the gold nanosensors, will be designed to ensure high selectivity. Third, theoretical modeling of this sensor will be carried out with focus on optimization of the device for sensing; parameters such as dimension of the sensor elements and of the nanochannels will be correlated to flow profiles and biomolecular kinetics. In addition, it might also be interesting to look into the possibility to locally enhance the concentration

of target molecules using electrophoretic concentration in the pore regions.[66] This study will constitute the backbone for the identification of the most suitable biorecognition reaction to test the performances of this device. At this stage, the performances of such a sensor with respect to detection limit, rate of binding and sample consumption must then be investigated and correlated to competing technologies, such as surface plasmon resonance, quartz-crystal microbalance. It is also worth noting that the combination of the chips with cell-derived membranes that span the nanoscale apertures[67] could provide novel information in the study of membrane-protein controlled transport-mediated processes, potentially applicable as a drug-screening assay. Furthermore, the miniaturization potential of sensors based on nano-components could be explored with the aim to produce fully operational devices on a chip, e.g. by integrating both a light source and the detection element in the sensor presented in Paper I. A further extension of the work could include the integration of nanoplasmonics sensors with transducer principles based on impedance.[68–70] While nanoplasmonic-based signals derive from local changes in refractive index, impedance readout is based on the electrical properties of the surrounding media. This enables for simultaneous tracking of different phenomena in the same experiment. Moreover, the combination of optical and electrical readout is also suitable from a design point of view since the principles do not interfere significantly with each other.

Acknowledgments

First of all I would like to thank my supervisor Fredrik Höök for the fruitful discussions and for helping me find my way through these first two years. The project has been stimulating and challenging, and I have learnt much.

I would also like to thank:

My co-supervisor Magnus Jonsson for the daily support and the long skype sessions about the nano- part of my work: -plasmonics, -fabrication and, of course, -bananas

Justin Schneiderman, my other co-supervisor, for guiding my first steps in the field of impedance sensing

the co-authors for the discussions and the support throughout this work

the Nanofabrication Laboratory staff at MC2 for the training and all those precious tips that helped me along the way

the Biological Physics group for contributing to an enjoyable working atmosphere and for giving me the chance to meet such an intercultural mix of talented people

Beniamino, Matteo, Virginia, Valentina, Luigi, Alessandra, Orlando, Iginia per aver ricreato quella italianità che tutti abbiamo ripromesso a noi stessi di fuggire una volta trasferiti all'estero

Kim per esserci. La naturalezza e l'intensità di quello che stiamo vivendo sono di una bellezza rara.

Last but not least my family: Delia, Elena and Marcello.
Grazie di tutto. Il vostro supporto, la vostra guida e il vostro affetto sono stati fondamentali durante questo lungo percorso. Vi sento vicini anche se distanti qualche migliaia di chilometri. Vi voglio bene e vi sarò sempre grato per l'enorme opportunità che mi avete concesso.

References

[1] Lukosz, W. *Biosensors & bioelectronics* **6**, 215–225 (1991).

[2] Liedberg, B., Lundström, I., and Stenberg, E. *Sensors and Actuators B: Chemical* **11**, 63–72 (1993).

[3] Vo-Dinh, T., Houck, K., and Stokes, D. L. *Analytical chemistry* **66**(20), 3379–83 October (1994).

[4] Swann, M. J., Peel, L. L., Carrington, S., and Freeman, N. J. *Analytical biochemistry* **329**(2), 190–8 June (2004).

[5] Lu, Y., Liu, G. L., Kim, J., Mejia, Y. X., and Lee, L. P. *Nano letters* **5**(1), 119–24 January (2005).

[6] Updike, S. and Hicks, G. *Nature* **214**, 986–988 (1967).

[7] Yun, Y., Dong, Z., Shanov, V. N., and Schulz, M. J. *Nanotechnology* **18**(46), 465505 November (2007).

[8] Zhang, Y., Kim, H.-H., and Heller, A. *Analytical chemistry* **75**(13), 3267–9 July (2003).

[9] Ramanathan, K., Jönsson, B., and Danielsson, B. *Analytica chimica acta* **427**, 1–10 (2001).

[10] Xie, B., Mecklenburg, M., Danielsson, B., Öhman, O., Norlin, P., and Winquist, F. *Analyst* **120**(January), 155–160 (1995).

[11] Graham, D. L., Ferreira, H., Bernardo, J., Freitas, P. P., and Cabral, J. M. S. *Journal of Applied Physics* **91**(10), 7786 (2002).

[12] De Palma, R., Reekmans, G., and Liu, C. *Analytical Chemistry* **79**(22), 8669–8677 (2007).

[13] Höök, F., Rodahl, M., Kasemo, B., and Brzezinski, P. *Proceedings of the* **95**(21), 12271–6 October (1998).

[14] Storri, S., Santoni, T., Minunni, M., and Mascini, M. *Biosensors & bioelectronics* **13**(3-4), 347–57 March (1998).

[15] Sung, J. H., Ko, H. J., and Park, T. H. *Biosensors & bioelectronics* **21**(10), 1981–6 April (2006).

[16] Woodbury, R. G., Wendin, C., Clendenning, J., Melendez, J., Elkind, J., Bartholomew, D., Brown, S., and Furlong, C. E. *Biosensors & bioelectronics* **13**(10), 1117–26 November (1998).

[17] Jonsson, M. P., Dahlin, A. B., Feuz, L., Petronis, S., and Höök, F. *Analytical chemistry* **82**(5), 2087–94 March (2010).

[18] De Angelis, F., Gentile, F., Mecarini, F., Das, G., Moretti, M., Candeloro, P., Coluccio, M., Cojoc, G., Accardo, A., Liberale, C., and Others. *Nature Photonics* **5**(September), 2–7 (2011).

[19] Newman, J. D. and Turner, A. P. F. *Biosensors & bioelectronics* **20**(12), 2435–2453 June (2005).

[20] Bangs, L. B. *Pure and Applied Chemistry* **68**(10), 1873–1879 (1996).

[21] Weeman, B. V. and Schuurs, A. *FEBS Letter* **15**(3), 232–236 (1971).

[22] Cheng, S., Fockler, C., Barnes, W. M., and Higuchi, R. *Proceedings of the National Academy of Sciences of the United States of America* **91**(12), 5695–9 June (1994).

[23] Kulasingam, V. and Diamandis, E. P. *Nature clinical practice. Oncology* **5**(10), 588–599 October (2008).

[24] Reichlin, T., Hochholzer, W., Bassetti, S., Steuer, S., Stelzig, C., Hartwiger, S., Biedert, S., Schaub, N., Buerge, C., Potocki, M., Noveanu, M., Breidthardt, T., Twerenbold, R., Winkler, K., Bingisser, R., and Mueller, C. *The New England journal of medicine* **361**(9), 858–67 August (2009).

[25] Ewers, M., Mielke, M. M., and Hampel, H. *Experimental gerontology* **45**(1), 75–79 January (2010).

[26] Friguet, B., Chaffotte, A. F., Djavadi-Ohaniance, L., and Goldberg, M. E. *Journal of Immunological Methods* **77**(2), 305–319 (1985).

[27] Haes, A., Hall, W., Chang, L., and Klein, W. *Nano Letters* (2004).

[28] Mayer, K., Lee, S., Liao, H., Rostro, B., and Fuentes, A. *Acs Nano* **2**(4), 687–692 (2008).

[29] Gunnarsson, A., Jönsson, P., Marie, R., Tegenfeldt, J. O., and Höök, F. *Nano letters* **8**(1), 183–8 January (2008).

[30] Haes, A., Zou, S., Schatz, G., and Van Duyne, R. *The Journal of Physical Chemistry B* **108**(1), 109–116 (2004).

[31] Feuz, L., Jonsson, M. P., and Höök, F. *Nano letters* **12**(2), 873–9 February (2012).

[32] Feuz, L., Jönsson, P., Jonsson, M. P., and Höök, F. *ACS nano* **4**(4), 2167–77 April (2010).

[33] Marko-Varga, G. A., Nilsson, J., and Laurell, T. *Electrophoresis* **25**(21-22), 3479–91 November (2004).

[34] Gervais, T. and Jensen, K. F. *Chemical Engineering Science* **61**(4), 1102–1121 February (2006).

[35] Bishop, J., Blair, S., and Chagovetz, a. *Biosensors & bioelectronics* **22**(9-10), 2192–8 April (2007).

[36] Hu, G., Gao, Y., and Li, D. *Biosensors & bioelectronics* **22**(7), 1403–9 February (2007).

[37] Faraday, M. *Philosopical Transaction of the Royal Society of London* **147**, 145–181 (1857).

[38] Mie, G. *Annalen der Physik* (1908).

[39] Stewart, M. E., Anderton, C. R., Thompson, L. B., Maria, J., Gray, S. K., Rogers, J. a., and Nuzzo, R. G. *Chemical reviews* **108**(2), 494–521 March (2008).

[40] Wooten, F. *No Optical Properties of Solids*. (1972).

[41] Kittel, C. *Introduction to Solid State Physics*. John Wiley & Sons, seventh ed edition, (2004).

[42] Link, S., Mohamed, M. B., and El-Sayed, M. a. *The Journal of Physical Chemistry B* **103**(16), 3073–3077 April (1999).

[43] Yu, Y.-Y., Chang, S.-S., Lee, C.-L., and Wang, C. R. C. *The Journal of Physical Chemistry B* **101**(34), 6661–6664 August (1997).

[44] Nordlander, P. *ACS nano* **3**(3), 488–92 March (2009).

[45] Aizpurua, J., Hanarp, P., Sutherland, D., Käll, M., Bryant, G., and García de Abajo, F. *Physical Review Letters* **90**(5), 5–8 February (2003).

[46] Bukasov, R. and Shumaker-Parry, J. S. *Nano letters* **7**(5), 1113–8 May (2007).

[47] Rochholz, H., Bocchio, N., and Kreiter, M. *New Journal of Physics* **9**(3), 53–53 March (2007).

[48] Futamata, M., Maruyama, Y., and Ishikawa, M. *The Journal of Physical Chemistry B* **107**, 7607–7617 (2003).

[49] Draine, B. T. and Flatau, P. J. *Journal of the Optical Society of America A* **11**(4), 1491 April (1994).

[50] Lal, S., Link, S., and Halas, N. J. *Nature Photonics* **1**(11), 641–648 November (2007).

[51] Dahlin, A. B., Chen, S., Jonsson, M. P., Gunnarsson, L., Käll, M., and Höök, F. *Analytical chemistry* **81**(16), 6572–80 August (2009).

[52] Dahlin, A., Tegenfeldt, J., and Höök, F. *Analytical chemistry* **78**(13), 4416–4423 (2006).

[53] Kelly, K., Coronado, E., Zhao, L., and Schatz, G. *The Journal of Physical Chemistry B* **107**, 668–677 (2003).

[54] Liedberg, B., Nylander, C., and Lundström, I. *Sensors and Actuators* **4**, 299–304 (1983).

[55] Michielin, O., Ramsden, J. J., and Vergères, G. *Biochimica et biophysica acta* **1375**(1-2), 110–6 October (1998).

[56] Hanarp, P., Sutherland, D., Gold, J., and Kasemo, B. *Colloids and Surfaces A: Physicochemical and Engineering Aspects* **214**(1-3), 23–36 March (2003).

[57] Autumn, K., Liang, Y. a., Hsieh, S. T., Zesch, W., Chan, W. P., Kenny, T. W., Fearing, R., and Full, R. J. *Nature* **405**(6787), 681–5 June (2000).

[58] Marmur, A. *Langmuir* (20), 3517–3519 (2004).

[59] Geim, A. K., Dubonos, S. V., Grigorieva, I. V., Novoselov, K. S., Zhukov, A. A., and Shapoval, S. Y. *Nature materials* **2**(7), 461–3 July (2003).

[60] Pendry, J. *Contemporary Physics* **45**(3), 191–202 May (2004).

[61] Müller, D. J., Schabert, F. a., Büldt, G., and Engel, a. *Biophysical journal* **68**(5), 1681–6 May (1995).

[62] Campbell, S. *The Science and Engineering of Microelectronic Fabrication*. Oxford University Press, second edi edition, (2001).

[63] Warren, J., Adams, D. P., Aziz, M. J., Link, C., Moberlychan, W. J., David, P., Hobler, G., and Schenkel, T. *MRS Bullettin* **32**(5), 424–432 (2007).

[64] Bratton, D., Yang, D., Dai, J., and Ober, C. K. *Polymers for Advanced Technologies* **17**(2), 94–103 February (2006).

[65] Fredriksson, H., Alaverdyan, Y., Dmitriev, a., Langhammer, C., Sutherland, D., Zäch, M., and Kasemo, B. *Advanced Materials* **19**(23), 4297–4302 December (2007).

[66] Hall, A. R., van Dorp, S., Lemay, S. G., and Dekker, C. *Nano letters* **9**(12), 4441–5 December (2009).

[67] Jönsson, P., Jonsson, M. P., and Höök, F. *Nano letters* **10**(5), 1900–6 May (2010).

[68] Huang, Y., Bell, M. C., and Suni, I. I. *Analytical chemistry* **80**(23), 9157–61 December (2008).

[69] Liao, W. and Cui, X. T. *Biosensors & bioelectronics* **23**(2), 218–24 September (2007).

[70] Varshney, M., Li, Y., Srinivasan, B., and Tung, S. *Sensors and Actuators B: Chemical* **128**(1), 99–107 December (2007).